

# Synthesis and Characteristics of Nickel Doped Barium M-Hexaferrite ( $\text{BaFe}_{12}\text{O}_{19}$ ) by Coprecipitation Method

Susilawati<sup>1\*</sup>, Aris Doyan<sup>1</sup>, Munib<sup>1,2</sup>

<sup>1</sup> Master of Science Education Study Program, Postgraduate University of Mataram, Mataram, Indonesia.

<sup>2</sup> Doctoral of Science Education Study Program, Postgraduate University of Mataram, Mataram, Indonesia.

Received: February 28, 2025

Revised: March 27, 2025

Accepted: April 25, 2025

Published: April 30, 2025

Corresponding Author:

Susilawati

[Susilawatihambali@unram.ac.id](mailto:Susilawatihambali@unram.ac.id)

© 2025 The Authors. This open access article is distributed under a (CC-BY License)



**Abstract:** Barium M-hexaferrite ( $\text{BaFe}_{12}\text{O}_{19}$ ) as an absorber of microwaves has been synthesized by coprecipitation method and its effect on changes in temperature and dopant substitution. Basic materials used in the synthesis of  $\text{BaCO}_3$ ,  $\text{FeCl}_3 \cdot 6\text{H}_2\text{O}$  and nickel metal. This study used a variation of calcination temperature of 80 °C, 400 °C, 600 °C and 800 °C for 4 hours with a variety of dopants 0; 0.4; 0.7 and 0.9. The results indicate that the formation of single phase and uniform distribution on M-barium hexaferrite ( $\text{BaFe}_{12-x}\text{Ni}_x\text{O}_{19}$ ) at 800 °C calcination temperature and variations in dopant  $x = 0.7$ . The elements of barium is spread very evenly matched with the concentration of each element in the compound  $\text{BaFe}_{12-x}\text{Ni}_x\text{O}_{19}$ . The addition of the dopant concentration can increase the value of conductivity that is in the range of  $10^{-6}$  to  $10^{-4}$  with a coercivity value at  $x = 0.7$  and calcination temperature of 800 °C at 0.05 T and magnetization value of 2.25 emu /g.

**Keywords:** Barium M-hexaferrite; Coprecipitation method; Dopant ion; Nickel.

## Introduction

The development of materials as microwave absorbers used as Radar Absorbing Material (RAM) which can absorb radar waves (Radio Detection and Ranging) (Susilawati et al., 2023). The material can be in the form of iron sand which can be utilized in high-tech applications. Microwave absorbers consist of two components, dielectric absorbers and magnetic absorbers (Syamsir, 2012).

One of the materials that are widely developed at this time is magnetic material which can be seen from its very complicated structure because the material can be characterized in various criteria including physical properties in the form of electrical, magnetic and optical properties (Hossain et al., 2022). Ferromagnetic nanocrystal material is a material that has been widely studied in recent years. The material that is often used is the ferrite group, one of which is hexagonal ferrite oxide (Dhiman et al., 2021).

Barium Hexaferrite has a stoichiometry with a stable hexagonal structure which is a ferromagnetic

oxide with dielectric and magnetic properties that are widely used in RF (Radio Frequency) and microwave applications. Barium Hexaferrite (BaM) is grouped into six types based on its chemical formula and crystal structure, namely M ( $\text{BaFe}_{12}\text{O}_{19}$ ), Y ( $\text{BaMe}_2\text{Fe}_{12}\text{O}_{22}$ ), W ( $\text{BaMe}_2\text{Fe}_{16}\text{O}_{27}$ ), Z ( $\text{Ba}_3\text{Me}_2\text{Fe}_{24}\text{O}_{41}$ ), X ( $\text{Ba}_2\text{Me}_2\text{Fe}_{28}\text{O}_{46}$ ) and U ( $\text{Ba}_4\text{Me}_2\text{Fe}_{36}\text{O}_{60}$ ) (Verma & Jasrotia, 2023). M, Y, W, Z, X, and U indicate the type of barium hexaferrite which is determined by the amount of iron and oxygen ions in the compound. While Me indicates a variable that can be replaced with Zn, Ti, Co, Ga, Al ions, and other metal cations of almost the same size according to the desired properties.

The electrical and magnetic properties of barium substitution Hexaferrite are highly dependent on the synthesis conditions due to the imbalance of charge distribution in the multivalent cation substitution process (Rajenimbalkar et al., 2024). The magnetic material barium M-hexaferrite (BaM) has a large anisotropic crystal and a resonance location that can be modified over a wide frequency range through ion substitution in hexaferrite and is soft with a relatively

## How to Cite:

Susilawati, S., Doyan, A., & Munib, M. (2025). Synthesis and Characteristics of Nickel Doped Barium M-Hexaferrite ( $\text{BaFe}_{12}\text{O}_{19}$ ) by Coprecipitation Method. *Journal of Material Science and Radiation*, 1(1), 29-35. Retrieved from <https://journals.balaipublikasi.id/index.php/jmsr/article/view/364>

large permeability and has a high saturation magnetic polarization and consists of strong anisotropic uniaxial crystals, high Curie temperature and large coercive field (Bartolomé et al., 2011).

With the presence of a very large coercive field, the anisotropic properties of the material increase so that its absorption properties become weaker, thus reducing the anisotropic properties, doping is required (Solizoda et al., 2024). Doping in this study in the formation of BaFe<sub>12</sub>O<sub>19</sub> is Ni by varying the calcination temperature and doping used to produce BaFe<sub>12-x</sub>Ni<sub>x</sub>O<sub>19</sub>.

## Method

The basic material of barium carbonate (BaCO<sub>3</sub>) is dissolved with HCl and FeCl<sub>3</sub> is dissolved with water. After that, the results of the two solutions are mixed and added with doping material in the form of pure nickel elements in liquid form with 20000 ppm which is then reacted with NH<sub>4</sub>OH to make the mixture into a precipitate. The process of reacting these materials is called the coprecipitation method, which is one of the inorganic compound synthesis methods based on the precipitation of more than one substance together when passing the saturation point. In the formation of barium ferrite substitution BaFe<sub>12-x</sub>Ni<sub>x</sub>O<sub>19</sub>, using variations of x = 0; 0.4; 0.7; and 0.9 at sintering temperatures of 32°C, 400°C, 600°C and 800°C (Susilawati et al., 2015).

Schematically, the research procedure process is shown in Figure 1 below:

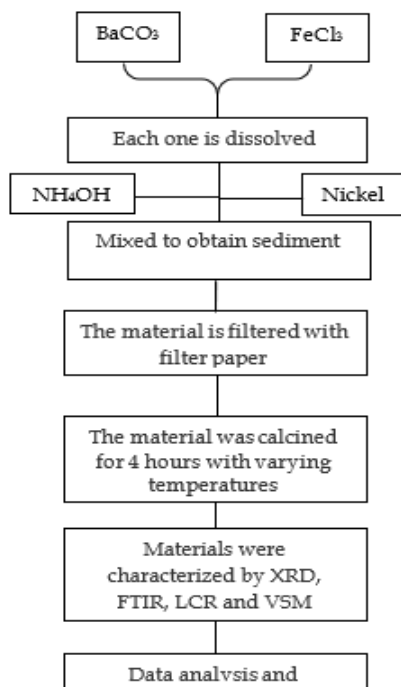


**Figure 1.** Process Flow of Barium M-hexaferrite BaFe<sub>12-x</sub>Ni<sub>x</sub>O<sub>19</sub> Synthesis by Coprecipitation Method

## Result and Discussion

### Result

Changes in calcination temperature and concentration of variable x show a tendency for color changes in the synthesized powder along with increasing temperature and dopant ions as shown in Figure 2.

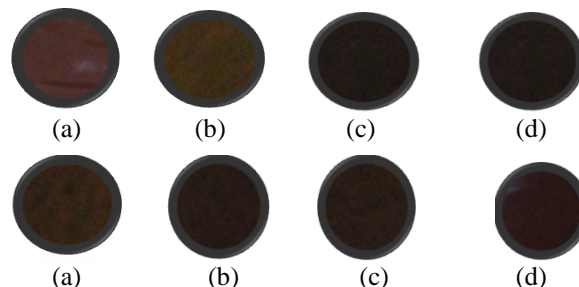


**Figure 2.** The effect of calcination temperature and variable x on the color change of BaFe<sub>12-x</sub>Ni<sub>x</sub>O<sub>19</sub> powder

Based on Figure 2, it is obtained that at the same calcination temperature by increasing the concentration of dopant ions, the color of the powder changes to blackish brown. At temperatures above 800°C, there is a tendency to be blackish brown, indicating that all the H<sub>2</sub>O and HCl elements are 100% gone (Susilawati et al., 2015). This indicates that in the heating process, the basic material BaCO<sub>3</sub> dissolved with HCl undergoes a perfect process. Meanwhile, with the same concentration of dopant ions and increasing calcination temperature, the color of the powder obtained is increasingly blackish brown (Sangwong et al., 2019).

**Table 1.** Peak XRD Results

2-theta(deg)	Phase Name	Chemical Formula
24.22(2)	Unknow	Unknow
27.9302	Barium Iron Oxide (2,2,0)	Ba <sub>3</sub> FeO <sub>5</sub>
28.5287	Unknow	Unknow
31.6708	Nickel Oxide (1,0,0)	Ni <sub>1,334</sub> O <sub>2</sub>
31.9202	Barium Iron Oxide (0,2,2) Nickel Oxide (0,0,2)	Ba <sub>3</sub> FeO <sub>5</sub> Ni <sub>1,334</sub> O <sub>2</sub>
33.238(7)	Barium Iron Oxide (1,2,2)	Ba <sub>3</sub> FeO <sub>5</sub>
35.687(7)	Unknow	Unknow
49.528(14)	Barium Iron Oxide (2,4,1)	Ba <sub>3</sub> FeO <sub>5</sub>
62.49(2)	Barium Iron Oxide (1,1,5)	Ba <sub>3</sub> FeO <sub>5</sub>

### XRD Analysis

Barium M-hexaferrite powder at variation x = 0.4 with calcination temperature of 800°C to form BaFe<sub>11.6</sub>Ni<sub>0.4</sub>O<sub>19</sub> was tested with XRD to determine the substitution of Ni dopant. XRD used in testing this sample used wavelength 1,541862 Å with Rigaku SmartLab brand which was tested at LIPI Fisika Serpong

Tangerang Selatan. Given the atomic radius is almost the same so it cannot change the structure of the basic material, but only causes a slight shift in the peak position of the diffraction pattern (angle  $2\theta$ ). The effect of substitution is very small as shown in Figure 3.

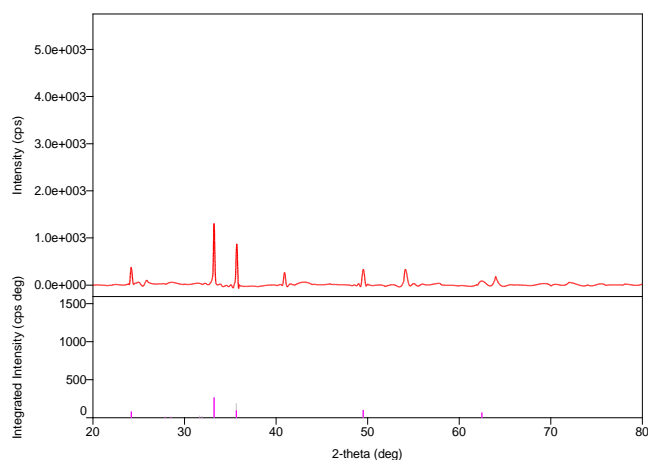


**Figure 3.** XRD pattern  $x=0.4$  and temperature  $800\text{ }^{\circ}\text{C}$  ( $\text{BaFe}_{11.6}\text{Ni}_{0.4}\text{O}_{19}$ )

Based on Figure 3 and Table 1, the X-ray diffraction pattern with the addition of nickel dopant concentration of 0.4 shows a peak at an angle of  $31.6708\text{ deg}$  containing a foreign phase after the addition of nickel oxide and at an angle of  $31.9202\text{ deg}$  there is a peak containing barium iron nickel oxide. The addition of dopant concentration results in foreign peaks which are compounds of the dopant (Mulyawan et al., 2021).

A more stable diffraction pattern occurs after the decomposition of the phase transformation at a temperature of  $840\text{ }^{\circ}\text{C}$  with a concentration of  $x = 0.4$  so that a fairly stable single phase is formed (Solizoda et al., 2024). The barium M-hexaferite phase is formed at high temperatures ( $T \geq 500\text{ }^{\circ}\text{C}$ ) and a single phase is formed, namely the hematite phase (Ramlan & Puspita, 2023). In addition, barium M-hexaferite will form at a temperature of  $975\text{ }^{\circ}\text{C}$  with a doping concentration of less than  $x = 0.8$ .

#### FTIR Analysis

To determine the occurrence of the doping process of Ni dopant on the crystal bond structure, Fourier Transform Infrared Spectroscopy (FTIR) analysis was used. The results of the analysis using FTIR on  $\text{BaFe}_{12-x}\text{Ni}_x\text{O}_{19}$  are shown in Figures 4 and 5.

Based on Figure 4, it was found that at the doping variation  $x = 0.7$ , there is a significant peak shift with the increasing calcination temperature. At the wavenumber  $1000\text{ cm}^{-1} - 1500\text{ cm}^{-1}$ , at the same concentration, there will be an increasing number of peaks with the rising calcination temperature, which are the absorption peaks of the base material indicating changes in bonding.

Meanwhile, at the wavenumber  $3400\text{ cm}^{-1}$ , it is the absorption of  $-\text{OH}$  where the higher the calcination temperature, the weaker the absorption becomes. This is because  $\text{H}_2\text{O}$  decreases as the calcination temperature increases.

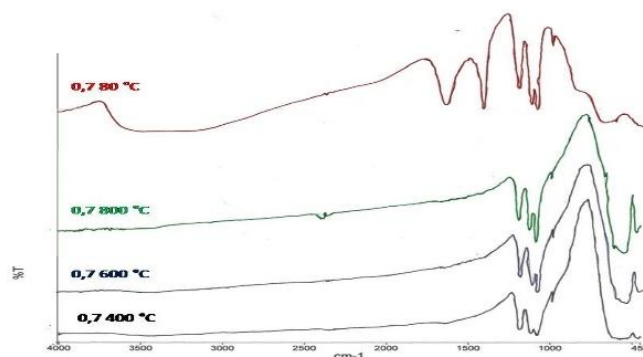


**Figure 4.** Absorption Pattern of  $\text{BaFe}_{12-x}\text{Ni}_x\text{O}_{19}$  in response to changes in calcination temperature at  $x = 0.7$

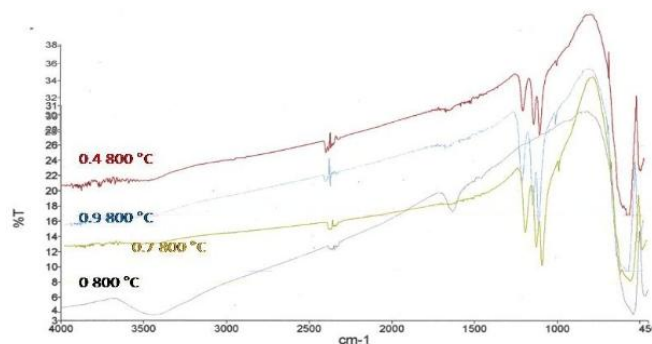


**Figure 5.** Absorption pattern of  $\text{BaFe}_{12-x}\text{Ni}_x\text{O}_{19}$  in response to changes in dopant ion concentration at  $T = 800\text{ }^{\circ}\text{C}$

Based on Figure 5, it is obtained that at wave numbers below  $600\text{ cm}^{-1}$ , with the increase in calcination temperature, the peaks tend to shift to the left. This indicates that at those wavenumbers, the metal  $\text{FeO}$  is present in the barium M-hexaferite or hematite phase. At a calcination temperature of  $T = 800\text{ }^{\circ}\text{C}$ , a significant peak shift occurs with increasing dopant concentration compared to other calcination temperatures. At the wavenumber  $1000\text{ cm}^{-1} - 1500\text{ cm}^{-1}$  at the same calcination temperature, there will be an increasing number of peaks with the rising dopant concentration, which are the absorption peaks of the base material. Meanwhile, at the wavenumber  $3400\text{ cm}^{-1}$ , it corresponds to the absorption of  $-\text{OH}$ , where the higher the concentration of dopant ions, the weaker the absorption becomes.

The characteristic of vibrations lower than  $600\text{ cm}^{-1}$ , which are the bonds between oxygen atoms and metal ions ( $\text{M-O}$ ), and their peaks increasingly found in the range of  $800 - 1500\text{ cm}^{-1}$  indicate the absorption peaks of the  $\text{BaCO}_3$  base material, while the absorption in the



range of  $2151.35 - 2923.88 \text{ cm}^{-1}$  represents OH absorption (Kubisiak et al., 2025). The absorption of OH falls within the range of  $3640 \text{ cm}^{-1}$  and the range of  $600 - 1650 \text{ cm}^{-1}$ , showing increasingly prominent peaks that indicate the absorption of the base material (Temuujin et al., 2004). The vibrational characteristics at  $450 \text{ cm}^{-1}$  and  $570 \text{ cm}^{-1}$  are the characteristics of the Fe-O bond, which are characteristic of Ba ferrite (Ting & Wu, 2010).

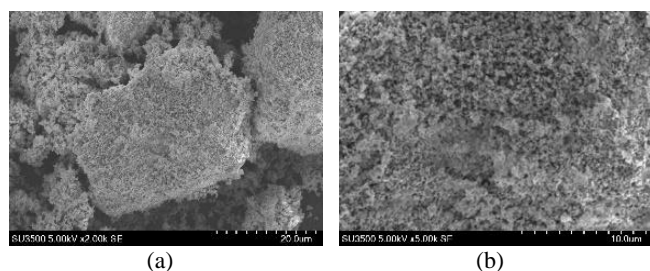


**Figure 6.** SEM photo of  $\text{BaFe}_{12-x}\text{Ni}_x\text{O}_{19}$  at  $x=0.9$  and  $T = 800^\circ\text{C}$  with magnification (a) 2000 and (b) 5000

#### SEM Analysis

To determine the distribution of elements contained in barium M-hexaferrite ( $\text{BaFe}_{12-x}\text{Ni}_x\text{O}_{19}$ ), an SEM-EDX tool was used. The characteristic data of the sample with Scanning Electron Microscopy (SEM) is obtained as shown in Figure 6.

Figure 6. SEM photo of  $\text{BaFe}_{12-x}\text{Ni}_x\text{O}_{19}$  at  $x=0.9$  and  $T = 800^\circ\text{C}$  with magnification (a) 2000 and (b) 5000 Based on Figure 6, the size of the powder is still difficult to determine because the powder is agglomerated and the range that can be clearly observed is still limited, as the particle dimensions of the powder have reached the nano scale. The increase in the size of the powder particles is in line with the increase in the variable concentration of dopant ions and the calcination temperature (Oliveira et al., 2023).

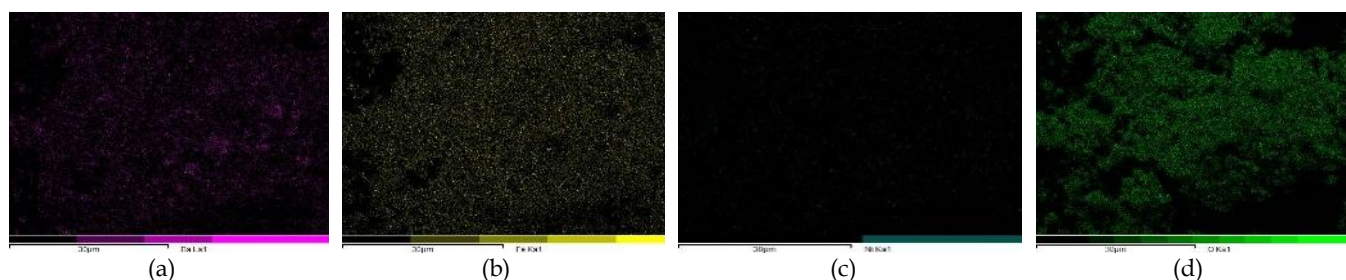


**Figure 7.** Distribution of Elements in  $\text{BaFe}_{12-x}\text{Ni}_x\text{O}_{19}$  at  $x=0.9$  and  $T = 800^\circ\text{C}$  (a) Ba (b) Fe (c) Ni and (d) O

The EDX elemental results of barium M-hexaferrite ( $\text{BaFe}_{12-x}\text{Ni}_x\text{O}_{19}$ ) show that the composition of barium M-hexaferrite contains the main elements Fe, Ba, C, O, and Ni. This is based on the observation of color backscatter as shown in Figure 7.

In Figure 7, it shows that the distribution of barium element content is very uniform according to the concentration of each element in the  $\text{BaFe}_{12-x}\text{Ni}_x\text{O}_{19}$  compound. This is consistent with the dispersion being

uniform according to the magnitude of the components present in BaM it self (Wang et al., 2022).

#### TEM Analysis

TEM analysis was used to qualitatively identify the dimensions of barium M-hexaferrite powder particles. The obtained TEM results are shown in the following Figure 8.

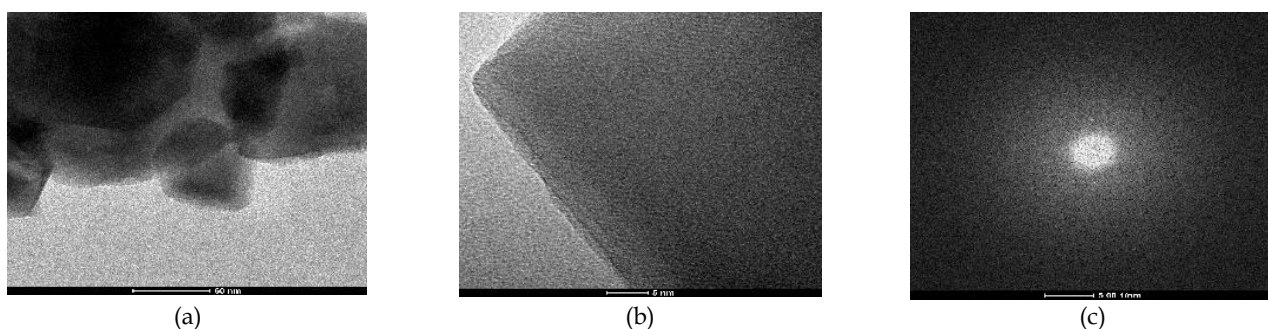


**Figure 8.** TEM photo at  $x = 0.7$  with  $T = 800^\circ\text{C}$

Based on Figure 8, it is clearly shown that the particle structure of BaM undergoes changes with the addition of dopant ions. At high temperatures and high doping concentrations, a structure with a hexagonal

shape will be formed (Peng et al., 2021). This is clearly seen in image 8 (a) which shows a particle size distribution similar to the crystal size with the smallest size reaching 20 nm, so it can be said that this material is

classified as a nanomaterial as shown in image 8 (b) with an order of about 5 nm.

Meanwhile, the distance between particles is clearly visible in Figure 8 (c), indicating that the particle size has reached the nano scale.

#### LCR Analysis

Measurement with an LCR meter of temperature variation with a constant concentration of  $x = 0.7$  yielded results as shown in Figure 9.

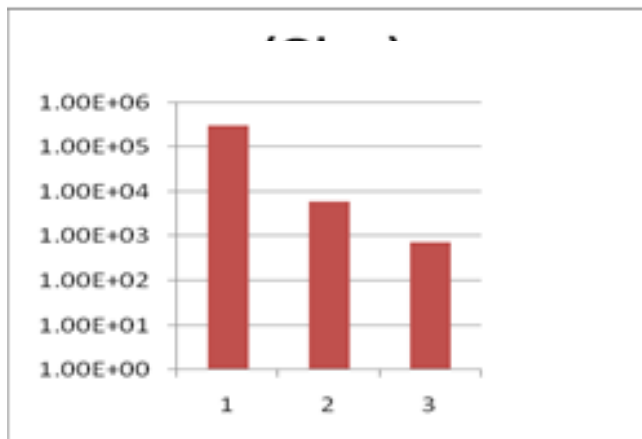


**Figure 9.** Resistivity Graph of Barium M-Hexaferrite ( $\text{BaFe}_{12-x}\text{Ni}_x\text{O}_{19}$ )

**Table 3.** Conductivity values

Concentration	X=0	X=0.7 400 °C	X=0.7 800 °C
Resistivity	3.19E+05	6.10E+03	7.37E+02
Diameter	1.17	1.174	1.17
Area	1.07	1.08	1.07
Thickness	3.94	3.3	3.14
Conductivity	1.01E-06	6.33E-05	5.51E-04

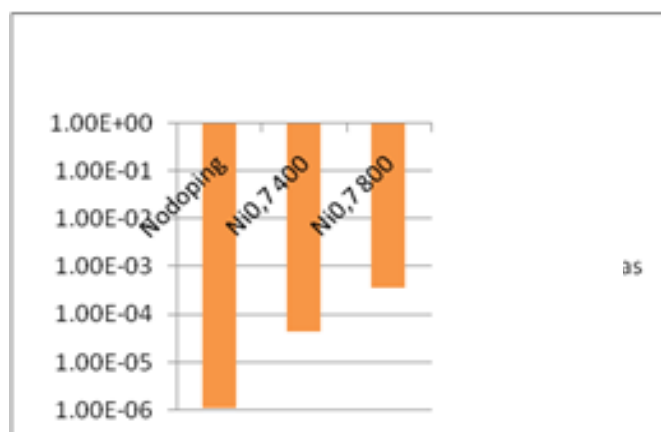


**Figure 10.** Conductivity Values of Barium M-Hexaferrite ( $\text{BaFe}_{12-x}\text{Ni}_x\text{O}_{19}$ )

From Table 3, it can be concluded that the higher the concentration of dopant ions, the higher the conductivity value. This conductivity is in the range of

$10^{-6}$  to  $10^{-4}$  (Figure 10). With the addition of dopant ions, the conductivity value increases (Godara et al., 2022).

#### VSM Analysis

The results of the synthesis of barium M-hexaferrite were characterized for their magnetic properties using a *vibrating sample magnetometer* (VSM) available at the Center for Advanced Material Science and Technology BATAN. The measurement results are in the form of a hysteresis curve showing the magnitude of magnetization (M) and coercivity (H) as shown in Figure 11.

Based on the literature, undoped barium M-hexaferrite ( $x = 0$ ) has a coercivity value of 0.0782 T and a magnetization value of 0.02 emu/gram. The characteristics of BaM have a coercivity value of 0.0005 T and a magnetization value of 0.02 emu/gram (Munib et al., 2016).

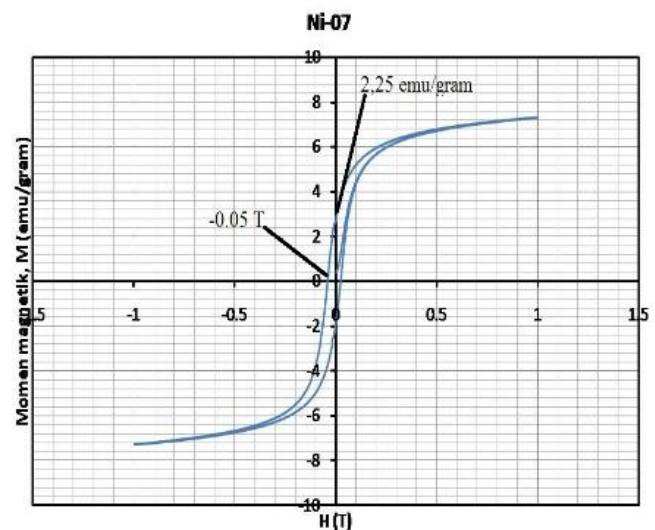


**Figure 11.** Hysteresis Curve at Calcination Temperature 800 °C at  $x = 0.7$

From Figure 11, it shows that the hysteresis curve of the barium M-hexaferrite sample with a dopant ion concentration of  $x = 0.7$  and a calcination temperature of 800 °C has a coercivity value of 0.05 T and a magnetization value of 2.25 emu/gram. This is larger compared to without doping ( $x = 0$ ). The best radar-absorbing material is found at low coercivity and high magnetization values, which are around 0.1104 T and 29 emu/gram at  $x = 0.4$  (Agustianto & Widyastuti, 2014). If it has a coercivity value of 0.0506 T and a magnetization value of 14.782 emu/gram at  $x = 0.3$  (Silvia et al., 2013).

Meanwhile, based on the heating duration, it was found that the coercivity value was 0.0082 T and the magnetization value was 0.55 emu/gram after 4 hours of heating (Sholihah & Zainuri, 2012). The higher the calcination temperature used, the higher the coercivity and magnetization values. At  $T < 800$  °C, the coercivity value is below 0.025 T and the magnetization is below 0.53 emu/gram. This indicates that in this study, with a

calcination temperature of  $T \geq 800\text{ }^{\circ}\text{C}$ , the coercivity value obtained was 0.05 T and the magnetization was 2.25 emu/gram.

## Conclusion

Based on the results and discussion, the M-hexaferrite barium powder has been successfully synthesized using the coprecipitation method with a diffraction pattern that is quite stable due to the presence of dopants at a temperature of  $800\text{ }^{\circ}\text{C}$  for 4 hours at  $x = 0.7$ , indicating the formation of a single phase. The elements of barium are evenly distributed according to the concentration of each element in the  $\text{BaFe}_{12-x}\text{Ni}_x\text{O}_{19}$  compound.

## Acknowledgements

The author team would like to thank all parties who have been involved and supported this research.

## Author Contributions

All authors contributed to writing this article.

## Funding

No external funding.

## Conflicts of Interest

No conflict interest.

## References

- Agustianto, R., & Widyastuti, W. (2014). Fraksi Mol Dan Variasi Ph Terhadap Sifat Magnetik Dan Struktur Mikro Barium Heksaferrit Dengan Metode Sol-Gel Auto Combustion. *Jurnal Teknik ITS*. <https://doi.org/10.12962/j23373539.v3i1.5861>
- Bartolomé, J., Arauzo, A., Kazak, N. V., Ivanova, N. B., Ovchinnikov, S. G., Knyazev, Y. V., & Lyubutin, I. S. (2011). Uniaxial magnetic anisotropy in  $\text{Co}_2\text{Fe}_{0.75}\text{O}_2\text{BO}_3$  compared to  $\text{Co}_3\text{O}_2\text{BO}_3$  and  $\text{Fe}_3\text{O}_2\text{BO}_3$ . *Physical Review B – Condensed Matter and Materials Physics*, 83(14), 144426. <https://doi.org/10.1103/PhysRevB.83.144426>
- Dhiman, P., Jasrotia, R., Goyal, D., & Mola, G. T. (2021). Hexagonal ferrites, synthesis, properties and their applications. *Mater. Res. Found*, 112, 336. <https://doi.org/10.21741/9781644901595-10>
- Godara, S. K., Kaur, V., Jasrotia, R., Thakur, S., Singh, V. P., Ahmed, J., Alshehri, S. M., Pandit, B., Singh, M., Kaur, P., & others. (2022). Effect of  $\text{Ca}^{2+}$  exchange at  $\text{Ba}^{2+}$  site on the structural, dielectric, morphological and magnetic traits of BaM nanohexaferrites. *Journal of Magnetism and Magnetic Materials*, 564, 170049. <https://doi.org/10.1016/j.jmmm.2022.170049>
- Hossain, M., Qin, B., Li, B., & Duan, X. (2022). Synthesis, characterization, properties and applications of two-dimensional magnetic materials. *Nano Today*, 42, 101338. <https://doi.org/10.1016/j.nantod.2021.101338>
- Kubisiak, P., Narkevičius, D., Nicotri, C., & Eilmes, A. (2025). Comparative study of isomeric TFSI and PFPSI anions in Li-ion electrolytes using quantum chemistry and Ab initio molecular dynamics. *The Journal of Physical Chemistry B*, 129(9), 2560–2572. <https://doi.org/10.1021/acs.jpcc.4c08414>
- Mulyawan, A., Winatapura, D. S., Sarwanto, Y., & Adi, W. A. (2021). Effects of La-Co substitution on the microstructure and magnetic properties of M-type barium ferrite. *AIP Conference Proceedings*, 2381(1). <https://doi.org/10.1063/5.0066280>
- Munib, Susilawati, & Savalas, L. R. T. (2016). Sintesis Barium M-hexaferrite ( $\text{BaFe}_{12-x}\text{Ni}_x\text{O}_{19}$ ) Doping Logam Nikel dengan Metode Kopresipitasi. *Jurnal Penelitian Pendidikan IPA*, 2(1). <https://doi.org/10.29303/jppipa.v2i1.28>
- Oliveira, T. G., Guerra, Y., Araujo-Barbosa, S., Gusmão, S. B. S., Lobo, A. O., Silva-Filho, E. C., Santos, F. E. P., Peña-Garcia, R., & Viana, B. C. (2023). Titanate nanotubes and their magnetic properties: Effect of ion exchange and calcination temperature. *Journal of Materials Research*, 38(5), 1332–1348. <https://doi.org/10.1557/s43578-023-00893-2>
- Peng, K., Zhou, Z., Wang, H., Wu, H., Ying, J., Han, G., Lu, X., Wang, G., Zhou, X., & Chen, X. (2021). Exceptional performance driven by planar honeycomb structure in a new high temperature thermoelectric material  $\text{BaAgAs}$ . *Advanced Functional Materials*, 31(24), 2100583. <https://doi.org/10.1002/adfm.202100583>
- Rajenimbalkar, R. S., Deshmukh, V. J., Patankar, K. K., & Somvanshi, S. B. (2024). Effect of multivalent ion doping on magnetic, electrical, and dielectric properties of nickel ferrite nanoparticles. *Scientific Reports*, 14(1), 29547. Retrieved from <https://www.nature.com/articles/s41598-024-81222-3>
- Ramlan, R., & Puspita, E. (2023). Effect of The Composition of  $\text{TiO}_2$  Additives on The Physical and Magnetic Properties Crystal Structure and Microstructure of  $\text{BaFe}_{12}\text{O}_{19}$  Magnetic Ceramics. *Indonesian Journal of Applied Physics*, 13(2), 207–214. <https://doi.org/10.13057/ijap.v13i2.5>
- Sangwong, N., Suwan, M., & Supothina, S. (2019). Effect of calcination temperature and dolomite or  $\text{Al}_2\text{O}_3$  doping on properties of NIR-reflective  $\text{CoFe}_2\text{O}_4$  black pigment. *Materials Today: Proceedings*, 17, 1595–1601. <https://doi.org/10.1016/j.matpr.2019.06.187>
- Sholihah, F. R., & Zainuri, M. (2012). Pengaruh Holding



- Time Kalsinasi Terhadap Sifat Kemagnetan Barium M-Hexaferrite ( $\text{BaFe}_{12-x}\text{Zn}_x\text{O}_{19}$ ) dengan Ion Doping Zn. *Jurnal Sains Dan Seni ITS*, 1(1), 15789. Retrieved from <https://www.neliti.com/publications/15789/pengaruh-holding-time-kalsinasi-terhadap-sifat-kemagnetan-barium-m-hexaferrite-b>
- Silvia, L., Rosyidah, K. C., & Zainuri, M. (2013). Pengaruh Ion Doping Zn pada Sifat Kemagnetan Barium M-Heksaferit  $\text{BaFe}_{12-x}\text{Zn}_x\text{O}_{19}$  berbasis Pasir Besi Tulungagung. *Jurnal Fisika Dan Aplikasinya*, 9(3), 121–124. <https://doi.org/10.12962/j24604682.v9i3.853>
- Solizoda, I. A., Zhivulin, V. E., Gudkova, S. A., Taskaev, S. V., Zabeivorota, N. S., Pesin, L. A., & Vinnik, D. A. (2024). Influence of the Substitution of Iron by Aluminum and Titanium on the Structure and Properties of Barium Hexaferrite. *Journal of Structural Chemistry*, 65(6), 1210–1218. <https://doi.org/10.1134/S002247662406009X>
- Susilawati, Doyan, A., Al-Qoyyim, T. M., Maemum, P. J., Ristanti, C. I., & Ariani, B. I. (2023). Synthesis of Barium M-Hexaferrite Using Co-precipitation Method with Zn Doping Based on Natural Iron Sand at Tebing Beach, North Lombok as Microwave Absorbent Material. *Jurnal Penelitian Pendidikan IPA*, 9(1), 498–503. <https://doi.org/10.29303/jppipa.v9i1.2935>
- Susilawati, S., Munib, M., & Doyan, A. (2015). Pengaruh Temperatur Kalsinasi Dan Subsitusi Logam Nikel Pada Pembentukan Fasa Barium M-Hexaferrite ( $\text{BaFe}_{12-x}\text{Ni}_x\text{O}_{19}$ ) Menggunakan FTIR. *Jurnal Pijar Mipa*, 10(1). <https://doi.org/10.29303/jpm.v10i1.14>
- Syamsir, A. (2012). Sintesis Nanokomposit  $\text{PAni}/\text{TiO}_2/\text{Karbon}$  Sebagai Penyerap Gelombang Mikro. *Jurnal Fisika Unand*, 1(1). Retrieved from <https://jfu.fmipa.unand.ac.id/index.php/jfu/article/view/9/0>
- Temuujin, J., Aoyama, M., Senna, M., Masuko, T., Ando, C., & Kishi, H. (2004). Synthesis of Y-type hexaferrites via a soft mechanochemical route. *Journal of Solid State Chemistry*, 177(11), 3903–3908. <https://doi.org/10.1016/j.jssc.2004.06.051>
- Ting, T.-H., & Wu, K.-H. (2010). Synthesis, characterization of polyaniline/ $\text{BaFe}_{12}\text{O}_{19}$  composites with microwave-absorbing properties. *Journal of Magnetism and Magnetic Materials*, 322(15), 2160–2166. <https://doi.org/10.1016/j.jmmm.2010.02.002>
- Verma, A., & Jasrotia, R. (2023). An overview of hard ferrites: types and structures. *Materials Research Foundations*, 142. Retrieved from <https://mrforum.com/product/9781644902318-1/>
- Wang, C., Zheng, Z., Zou, Y., & Feng, Q. (2022). Enhanced microstructure homogeneity, density and magnetic performances of the BaM hexaferrite/PDMS composite films through solvent-assisted synthesis. *Ceramics International*, 48(15), 22147–22152. <https://doi.org/10.1016/j.ceramint.2022.04.214>